Chapter 4

Imaging of Extended Objects with Finite Sources

The Fraunhofer diffraction equations derived in the last chapter assume self-luminous point objects. Photomasks used in optical lithography require illumination by light sources that are physically extended. In addition, we must generalize our imaging formulation to consider mask patterns that in reality have finite dimensions.

We begin this chapter by studying image formation of a finite object under coherent illumination (by a point source) in which the fields of all object points have a definite phase relationship with one another. We shall find that coherent imaging is characterized by a transfer function that is essentially the point spread function of the imaging system. For a photomask illuminated by a finite source, despite incoherence between source points making up the extended source, vibrations at different object points are correlated due to diffraction of the illumination optics. Analysis under such partially coherent imaging scenarios requires the concept of spatial coherence. Similar to the theory of temporal coherence (quasi-monochromatic light), we need to quantify the correlation of vibrations between two points as a function of their separation and of the characteristics of the light source. We shall learn that partially coherent imaging is characterized by a set of transmission cross-coefficients that is related to the coherent transfer function and the illumination configuration.

4.1 Coherent illumination

Since the relative phase between vibrations at any two object points is fixed under coherent illumination, we can characterize the imaging system by a transfer function $H_0(x'_o, y'_o; x_i, y_i)$, defined as the field at (x_i, y_i) on the image plane caused by an object source point at (x'_o, y'_o) with unit amplitude and zero phase. For a complex

field $U_o(x_o', y_o')$ on the object plane, the field on the image plane is

$$U_i(x_i, y_i) = \iint_{-\infty}^{+\infty} U_o(x_o', y_o') H_0(x_o', y_o'; x_i, y_i)\, dx_o' dy_o'. \tag{4.1}$$

We shall develop the relationship between $H_0(x_o', y_o'; x_i, y_i)$ and the point spread function of the system.

Consider a point source located at (x_o'', y_o''):

$$U_o(x_o', y_o') = \delta(x_o'' - x_o') \cdot \delta(y_o'' - y_o').$$

The field on the image plane is

$$U_i(x_i, y_i) = H_0(x_o'', y_o''; x_i, y_i). \tag{4.2}$$

But the field on the image plane arising from a point source at (x_o'', y_o'') is also given by the Fraunhofer diffraction formula. If we scale all object space dimensions by the lateral magnification M and furthermore reflect the x_o'-axis and the y_o'-axis with respect to the origin, such that an object point and its geometrical image have the same coordinates:[i]

$$x_o = -Mx_o' \qquad \text{and} \qquad y_o = -My_o',$$

the Fraunhofer diffraction formula of Eq. (3.20) becomes

$$U_i(x_i, y_i) = C_1 \iint_{-\infty}^{+\infty} \tilde{P}_0(\eta, \xi; x_o, y_o; x_i, y_i) e^{-i\frac{2\pi}{\lambda R}[\eta(x_i - x_o) + \xi(y_i - y_o)]}\, d\eta d\xi, \tag{4.3}$$

where C_1 is a constant and $\tilde{P}_0(\eta, \xi; x_o, y_o; x_i, y_i)$ is the *pupil function* that characterizes the aperture. Comparing Eq. (4.2) with Eq. (4.3) we can express the transfer function as

$$H_0(x_o, y_o; x_i, y_i) = C_1 \iint_{-\infty}^{+\infty} \tilde{P}_0(\eta, \xi; x_o, y_o; x_i, y_i) e^{-i\frac{2\pi}{\lambda R}[\eta(x_i - x_o) + \xi(y_i - y_o)]}\, d\eta d\xi.$$

Let us focus on optical systems of which the transfer function depends on the difference between the image and object coordinates $(x_i - x_o, y_i - y_o)$ but not on the

[i]For the optical system depicted in Fig. 2.7, the relationship between object and image coordinates is

$$x_o = M' x_o' \qquad \text{and} \qquad y_o = M' y_o',$$

where $M' < 0$. In this text, the lateral magnification M always denotes a positive quantity such that $M = |M'|$ (see footnote on p. 27).

Chapter 5

Resolution and Image Enhancement

It is natural, before using an optical imaging instrument, to understand its resolving power. Traditionally, resolution is a measure of the ability of an imaging system to separate images of two neighboring object points. Although, within the confines of geometrical optics, the image of a point is sharp, the actual image is smeared because of diffraction. When the diffraction patterns of two point objects overlap and their principal maxima draw closer, it becomes more difficult to distinguish the objects.

Hence there is no precise resolution limit because it depends on the recording medium. An approximate measure of resolution can be specified using the heuristic criterion of Rayleigh (J. W. Strutt) [20–22]. Images of two point objects of equal brightness are considered just resolved when the principal maximum of one coincides with the first minimum of the other. For an imaging system with a circular aperture that has a point spread function described by Eq. (3.23), the resolution according to Rayleigh's criterion is

$$0.61\frac{\lambda_0}{\mathrm{NA}}.$$

In optical lithography and integrated circuit fabrication, we are concerned not only with delineation of patterns that are placed closely with one another, but also with reliable replication of small features. To refine Rayleigh's criterion in order to distinguish between these two requirements, let us define *minimum half-pitch* as the measure of object denseness; and denote the smallest size of an individual feature by *minimum dimension*. Minimum dimension relates to the speed of a transistor, while minimum half-pitch determines transistor integration density.

Since imaging under partially coherent illumination is characterized by the mutual intensity, with the transmission cross-coefficient, defined by the pupil and illumination configuration, taking a role analogous to a frequency transfer function, we expect that the resolution is closely related to the transmission cross-coefficient.

In this chapter we examine the minimum half-pitch and dimension of an imaging system illuminated by a quasi-monochromatic extended source of mean wavelength $\overline{\lambda} = \lambda$ and a semi-aperture angle at the image plane of θ_{obj}. Our analysis focuses on circular pupils, the shape used exclusively in optical lithography. The analysis techniques, nevertheless, are applicable for pupils of general shapes.

5.1 Image intensity spectrum

Since minimum half-pitch measures denseness of patterns, it is determined by the image intensity frequency content. By Fourier transformation of Eq. (4.37) we obtain the spectrum of the image:

$$\begin{aligned}
\tilde{\hat{I}}(\hat{f},\hat{g}) &= \iint_{-\infty}^{+\infty} \hat{I}(\hat{x},\hat{y}) e^{+i2\pi(\hat{f}\hat{x}+\hat{g}\hat{y})}\, d\hat{x}d\hat{y} \\
&= \int_{-\infty}^{+\infty}\cdots\int TCC(\hat{f}',\hat{g}';\hat{f}'',\hat{g}'')\tilde{\hat{O}}(\hat{f}',\hat{g}')\tilde{\hat{O}}^*(\hat{f}'',\hat{g}'') \\
&\qquad e^{-i2\pi[(\hat{f}'-\hat{f}'')\hat{x}+(\hat{g}'-\hat{g}'')\hat{y}]}\, e^{+i2\pi(\hat{f}\hat{x}+\hat{g}\hat{y})}\, d\hat{f}'d\hat{g}'d\hat{f}''d\hat{g}''d\hat{x}d\hat{y} \\
&= \iiiint_{-\infty}^{+\infty} TCC(\hat{f}',\hat{g}';\hat{f}'',\hat{g}'')\tilde{\hat{O}}(\hat{f}',\hat{g}')\tilde{\hat{O}}^*(\hat{f}'',\hat{g}'') \\
&\qquad \delta(\hat{f}-\hat{f}'+\hat{f}'')\delta(\hat{g}-\hat{g}'+\hat{g}'')\, d\hat{f}'d\hat{g}'d\hat{f}''d\hat{g}'' \\
&= \iint_{-\infty}^{+\infty} TCC(\hat{f}+\hat{f}'',\hat{g}+\hat{g}'';\hat{f}'',\hat{g}'') \\
&\qquad \tilde{\hat{O}}(\hat{f}+\hat{f}'',\hat{g}+\hat{g}'')\tilde{\hat{O}}^*(\hat{f}'',\hat{g}'')d\hat{f}''d\hat{g}''. \qquad (5.1)
\end{aligned}$$

The image contains a frequency component $(\hat{f},\hat{g})$ only if there is another component $(\hat{f}'',\hat{g}'')$ such that

$$\begin{aligned}
&TCC(\hat{f}+\hat{f}'',\hat{g}+\hat{g}'';\hat{f}'',\hat{g}'') = \\
&\qquad \iint_{-\infty}^{+\infty} \tilde{\hat{J}}(\hat{p},\hat{q})\tilde{\hat{H}}(\hat{p}+\hat{f}+\hat{f}'',\hat{q}+\hat{g}+\hat{g}'')\tilde{\hat{H}}^*(\hat{q}+\hat{f}'',\hat{q}+\hat{g}'')\, d\hat{p}d\hat{q} \neq 0.
\end{aligned}$$

According to Fig. 4.8, this condition is satisfied if the effective source and the displaced pupils overlap. For circular apertures, Fig. 4.8 can be redrawn as Fig. 5.1. Since the radius of the pupil in normalized units is 1, the displaced coherent frequency transfer functions $\tilde{\hat{H}}(\hat{p}+\hat{f}+\hat{f}'',\hat{q}+\hat{g}+\hat{g}'')$ and $\tilde{\hat{H}}(\hat{p}+\hat{f}'',\hat{q}+\hat{g}'')$ can overlap only if

$$\sqrt{[(\hat{f}+\hat{f}'')-\hat{f}'']^2+[(\hat{g}+\hat{g}'')-\hat{g}'']^2} = \sqrt{\hat{f}^2+\hat{g}^2} = \hat{\rho} \leq 2.$$

Chapter 6

Oblique Rays

We have, so far, treated light as a scalar quantity. Such treatment is adequate for light traveling at shallow angles with respect to the optic axis. At larger angles we need to consider the vector nature of light vibrations. Our investigations are concerned with the electric field vector only, since, as Otto Wiener demonstrated in his 1890 experiment, photochemical action is related to the electric rather than the magnetic vector.[i]

6.1 Polarization

Consider a time-harmonic plane wave traveling in the z-direction:

$$U(z,t) = Ae^{+i(kz-\omega t)}.$$

Since the electric field vector is perpendicular to the propagation direction [see Eq. (1.25)], we can express the electric field as

$$\begin{aligned} E_x &= a_x e^{+i(\phi_x + kz - \omega t)}, \\ E_y &= a_y e^{+i(\phi_y + kz - \omega t)}, \\ E_z &= 0. \end{aligned} \tag{6.1}$$

[i]Dependence on the electric but not the magnetic vector is a consequence of electromagnetic theory. Photoresist exposure is an ionization process in which an electron is released from an atomic bond. The electromagnetic force on a charged particle at rest is proportional to the electric vector according to the *Lorentz law*:

$$\mathbf{F} = q\big(\mathbf{E} + \mathbf{v} \times \mathbf{B}\big). \tag{1.10}$$

Quantum mechanically, the ionization process is a result of electron-photon interaction at optical frequencies that excites the system from one energy eigenstate to another. At such frequencies the electric dipole approximation is valid and the interaction Hamiltonian H involves only the electric field [41]:

$$H = q\mathbf{r} \cdot \mathbf{E}.$$

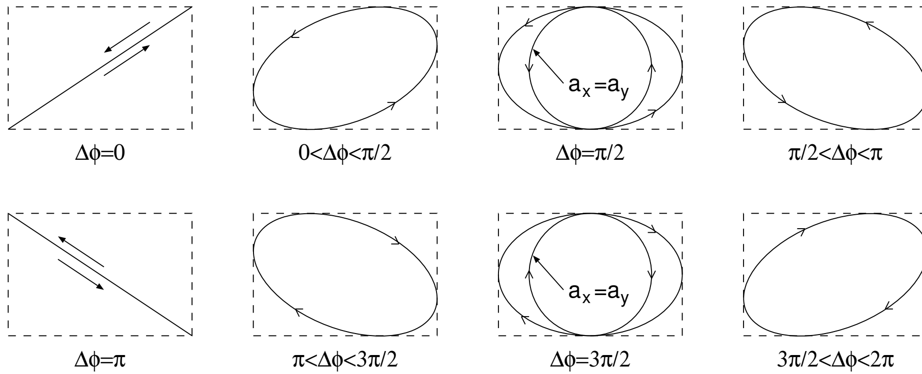

Figure 6.1: Linear polarization $(\Delta\phi = n\pi, n \in \mathbf{Z})$ and circular polarization $(a_x = a_y, \Delta\phi = (2n+1)\pi/2, n \in \mathbf{Z})$ are special cases of elliptic polarization.

If we pick an arbitrary point and observe the trajectory of the end-point of the electric field vector, its locus is, in general, an ellipse (see Exercise 6.1). The field is *elliptically polarized*. In the special case where

$$\Delta\phi = \phi_y - \phi_x = n\pi, \quad n \in \mathbf{Z},$$

$$\frac{E_y}{E_x} = (-1)^n \frac{a_y}{a_x}. \tag{6.2}$$

The field is *linearly polarized*. The electric field vector vibrates back and forth along a straight line. In the other special situation of *circularly polarized* light, the amplitudes and phases of E_x and E_y are related by

$$a_x = a_y \qquad \text{and} \qquad \phi_y - \phi_x = \frac{(2n+1)\pi}{2}, \quad n \in \mathbf{Z}.$$

The trajectory of the end-point of the electric field vector is a circle. These polarization states are illustrated in Fig. 6.1.

Although monochromatic light is always polarized, vibrations of the electric and magnetic vectors in a field produced by a quasi-monochromatic extended source is generally neither *polarized* (completely regular) nor *unpolarized* (totally irregular). They are *partially polarized*. Similar to the concept of spatial coherence in which the vibrations at two points are somewhat correlated (see §4.3.1), field-vector vibrations of partially polarized light are somewhat regular. The extent of regularity is characterized by the *degree of polarization*.

To determine the polarization properties of light, consider a quasi-monochromatic wave propagating in the z-direction. The electric field vector at an arbitrary point is

$$E_x(t) = a_x(t)e^{+i[\phi_x(t)-\overline{\omega}t]} \qquad \text{and} \qquad E_y(t) = a_y(t)e^{+i[\phi_y(t)-\overline{\omega}t]}.$$

Chapter 7

Aberrations

We have, thus far, assumed the image-forming wavefronts to be spherical. As we understand from Chapter 2, the emerging wavefronts from the pupil are in general aspherical, even if the lens surfaces are spherical. Deviation of wavefronts from sphericity is called *aberration*.[i]

Within the domain of geometrical optics, an aberrated image can be examined by considering the intersection of aberrated rays with the image plane. Such treatment, adequate for instruments in which the aberrations are on the order of wavelengths, is known as the *Seidel theory of aberrations*. But the precision required of imaging systems in optical lithography means that the wave aberration is a small fraction of the wavelength. In this situation, the geometrical theory loses its validity; the Seidel treatment is insufficient. We need to study the effects of aberrations based on diffraction theory.

7.1 Diffraction of an aberrated wavefront

Consider the imaging scenario shown in Fig. 7.1, where a spherical wavefront W of uniform amplitude and of radius R converges toward its center P_0, which is defined as the origin. Let us denote the aberrated wavefront that intersects W at the center of the pupil by W', the points at which an imaging ray intersects W and W' by Q and Q', and the distance between Q and Q' measured along the ray by $\lambda\Phi_0$. According to the Huygens-Fresnel principle [Eq. (3.11)], the field at a point P in the neighborhood of P_0 is

$$U(P) = \iint_S \frac{e^{-ik(R-r_p)} e^{+i2\pi\Phi_0}}{Rr_p} \, dS. \tag{7.1}$$

[i]In addition to Born and Wolf [6], Mahajan [48] provides a detailed discussion on aberrations.

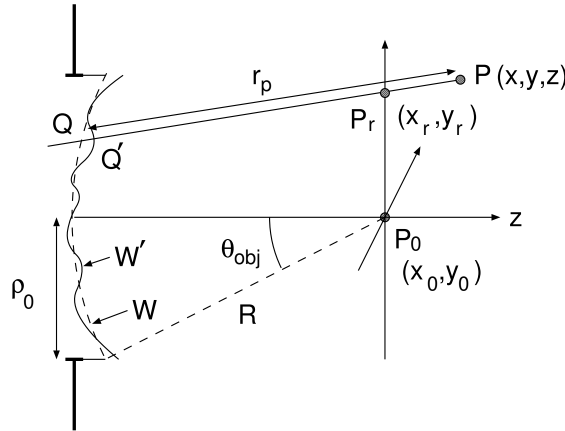

Figure 7.1: Diffraction of an aberrated wavefront.

Let (η, ξ, χ) be the coordinates of Q, let (x, y, z) be those of P, and denote the radius of the pupil by ρ_0. We also define the variables $(\hat{\rho}, \phi)$ and (r, ψ) such that

$$\begin{aligned} x &= r\cos\psi, & y &= r\sin\psi, \\ \eta &= \rho_0\hat{\rho}\cos\phi, & \xi &= \rho_0\hat{\rho}\sin\phi. \end{aligned}$$

Since Q lies on the spherical wavefront,

$$\chi = -\sqrt{R^2 - (\rho_0\hat{\rho})^2} = -R\Big[1 - \frac{(\rho_0\hat{\rho})^2}{2R^2} + \cdots\Big].$$

If $R \gg \rho_0$ and $R \gg \sqrt{x^2+y^2+z^2}$, we can make the approximation (see Exercise 7.1)

$$\begin{aligned} -k(R - r_p) &\approx \frac{2\pi}{\lambda}\frac{x\eta + y\xi + z\chi}{R} \\ &\approx \frac{2\pi}{\lambda}\bigg\{-z\Big[1 - \frac{(\rho_0\hat{\rho})^2}{2R^2}\Big] + \frac{\rho_0\hat{\rho}r}{R}\cos(\phi-\psi)\bigg\} \\ &= -2\pi\bigg[\hat{\rho}\hat{r}\cos(\phi-\psi) - \breve{z}\Big(\frac{1}{\sin^2\theta_{\text{obj}}} - \frac{\hat{\rho}^2}{2}\Big)\bigg], \end{aligned} \tag{7.2}$$

where

$$\begin{aligned} \hat{x} &= \frac{x}{\lambda/\sin\theta_{\text{obj}}} = \frac{x}{\lambda_0/\text{NA}}, & \hat{y} &= \frac{y}{\lambda/\sin\theta_{\text{obj}}} = \frac{y}{\lambda_0/\text{NA}}, \\ \hat{r} &= \frac{r}{\lambda/\sin\theta_{\text{obj}}} = \sqrt{\hat{x}^2+\hat{y}^2}, & \breve{z} &= \frac{z}{\lambda/\sin^2\theta_{\text{obj}}}. \end{aligned} \tag{7.3}$$

Chapter 8

Numerical Computation

The theoretical developments in the last chapters have provided us with equations that describe optical imaging in photolithography. With these equations, images of objects can be computed in lieu of carrying out exposures. The possibility to *simulate* allows us to harness the power of affordable computers to predict images of object patterns, and to optimize the object and exposure configuration given a desired image. In this chapter we discuss common numerical formulations for imaging simulation.

8.1 Imaging equations

Summarizing results of previous chapters, the imaging equation for a system with lateral magnification M is [from Eqs. (6.14) and (6.68)]:

$$\hat{I}(\hat{x},\hat{y},z) = K \int_{-\infty}^{+\infty} \cdots \int \tilde{\hat{J}}(\hat{f},\hat{g})\tilde{\hat{H}}(\hat{f}+\hat{f}',\hat{g}+\hat{g}')\tilde{\hat{H}}^*(\hat{f}+\hat{f}'',\hat{g}+\hat{g}'')$$
$$\tilde{\hat{O}}(\hat{f}',\hat{g}')\mathbf{M}(\hat{f}+\hat{f}',\hat{g}+\hat{g}')\mathbf{E}_0 \cdot \tilde{\hat{O}}^*(\hat{f}'',\hat{g}'')\mathbf{M}^*(\hat{f}+\hat{f}'',\hat{g}+\hat{g}'')\mathbf{E}_0^*$$
$$e^{-i2\pi\varphi} d\hat{f} d\hat{g} d\hat{f}' d\hat{g}' d\hat{f}'' d\hat{g}''$$
$$= K \int_{-\infty}^{+\infty} \cdots \int \tilde{\hat{J}}(\hat{f},\hat{g})\tilde{\hat{H}}(\hat{f}+\hat{f}',\hat{g}+\hat{g}')\tilde{\hat{H}}^*(\hat{f}+\hat{f}'',\hat{g}+\hat{g}'')$$
$$\sum_{\substack{i=\{x,y\}\\ j=\{x,y\}\\ k=\{x,y,z\}}} M_{ik}(\hat{f}+\hat{f}',\hat{g}+\hat{g}')M_{jk}^*(\hat{f}+\hat{f}'',\hat{g}+\hat{g}'')E_i E_j^*$$
$$\tilde{\hat{O}}(\hat{f}',\hat{g}')\tilde{\hat{O}}^*(\hat{f}'',\hat{g}'')e^{-i2\pi\varphi} d\hat{f} d\hat{g} d\hat{f}' d\hat{g}' d\hat{f}'' d\hat{g}'', \quad (8.1)$$

where

$$K = \begin{cases} n_{\text{image}} & \text{for coupling image [see Eq. (6.14)]}, \\ n'_{\text{p}} & \text{for resist image [see Eq. (6.68)]}, \end{cases}$$

n_{image} is refractive index of image space,

n'_{p} is real part of resist refractive index,

$$\tilde{\hat{J}}(\hat{f},\hat{g}) \quad \text{is the effective source,} \tag{4.31}$$

$$\hat{H}(\hat{f},\hat{g}) = \begin{cases} \sqrt[4]{\frac{1-n^2_{\text{image}}M^2\hat{\rho}^2_\theta}{1-\hat{\rho}^2_\theta}}\, e^{+i2\pi\Phi(\hat{\rho},\phi)} & \text{if } \hat{\rho}_\theta \le \sin\theta_{\text{obj}}, \\ 0 & \text{otherwise,} \end{cases} \tag{6.69}$$

$$\Phi(\hat{\rho},\phi) = \sum_{j=1}^{J} c_j Z_j(\hat{\rho},\phi), \tag{7.10}$$

$$\mathbf{M}(\hat{f},\hat{g}) = \begin{cases} \mathbf{M}_0(\hat{f},\hat{g}) & \text{for coupling image [see Eq. (6.14)]}, \\ \mathbf{M}_{\text{stack}}(\hat{f},\hat{g}) & \text{for resist image [see Eq. (6.68)]}, \end{cases}$$

$$\mathbf{M}_0 = \begin{bmatrix} M_{0_{xx}} & M_{0_{yx}} \\ M_{0_{xy}} & M_{0_{yy}} \\ M_{0_{xz}} & M_{0_{yz}} \end{bmatrix} = \begin{bmatrix} P_{x\perp x} + P_{x\|x} & P_{y\perp x} + P_{y\|x} \\ P_{x\perp y} + P_{x\|y} & P_{y\perp y} + P_{y\|y} \\ P_{x\|z} & P_{y\|z} \end{bmatrix} \tag{6.13}$$

$$\begin{aligned} P_{x\perp x} &= \frac{\beta^2}{1-\gamma^2}, & P_{y\perp x} &= -\frac{\alpha\beta}{1-\gamma^2}, \\ P_{x\perp y} &= -\frac{\alpha\beta}{1-\gamma^2}, & P_{y\perp y} &= \frac{\alpha^2}{1-\gamma^2}, \\ P_{x\perp z} &= 0, & P_{y\perp x} &= 0, \end{aligned} \tag{6.10}$$

$$\begin{aligned} P_{x\|x} &= \frac{\alpha^2\gamma}{1-\gamma^2}, & P_{y\|x} &= \frac{\alpha\beta\gamma}{1-\gamma^2}, \\ P_{x\|y} &= \frac{\alpha\beta\gamma}{1-\gamma^2}, & P_{y\|y} &= \frac{\beta^2\gamma}{1-\gamma^2}, \\ P_{x\|z} &= -\alpha, & P_{y\|z} &= -\beta, \end{aligned} \tag{6.12}$$

$$\begin{aligned} \mathbf{M}_{\text{stack}} &= \begin{bmatrix} M_{S_{xx}} & M_{S_{yx}} \\ M_{S_{xy}} & M_{S_{yy}} \\ M_{S_{xz}} & M_{S_{yz}} \end{bmatrix} \\ &= \begin{bmatrix} F_\perp P_{x\perp x} + F_\|^{xy} P_{x\|x} & F_\perp P_{y\perp x} + F_\|^{xy} P_{y\|x} \\ F_\perp P_{x\perp y} + F_\|^{xy} P_{x\|y} & F_\perp P_{y\perp y} + F_\|^{xy} P_{y\|y} \\ F_\|^z P_{x\|z} & F_\|^z P_{y\|z} \end{bmatrix} \end{aligned} \tag{6.66}$$

Chapter 9

Variabilities

In replicating an integrated circuit layout during fabrication, the same object shapes are often delineated numerous times. Because of unavoidable variabilities of a manufacturing process, the delineated shapes are generally different from the nominal shapes and from one another. This variability should be kept under the specified tolerance according to which integrated circuits are designed. Too much deviation causes circuit failure.

An understanding of the various causes of variation is helpful in devising means to reduce, stabilize, and compensate for the undesirable variation. Although all processing steps (such as deposition, lithography, etching, and chemical-mechanical polishing) contribute to patterning nonuniformity, we focus on variabilities arising from optical imaging, since, with both layout shapes and image tolerance shrinking rapidly compared with λ_0/NA, control of image variabilities is of increasing concern. Lithography becomes more difficult with decreasing k_1 and $k_{1_{\text{half-pitch}}}$.

9.1 Categorization

We can classify the causes of lithography variability into two categories. One affects object shapes located in identical environments, and the other impacts the same object shapes situated within distinct configurations of neighboring shapes. Let us call the effects of the former *fluctuations* and those of the latter *inherent variations*. The same cause can result in both fluctuation and inherent variation. On the other hand, a fluctuation and an inherent variation may have similar manifestations.

To distinguish fluctuation from inherent variation we must first expound the meaning of environment. Let us define a *feature* as an object shape within a particular configuration of neighboring shapes. The shapes A and B in Fig. 9.1, although identical, are distinct features because their environments of shapes are different. The periodic space described by Eq. (5.5) is a feature that is fully specified by its foreground and background transmittance t_{fg} and t_{bg}, size $\hat{d}$, and period $\hat{p}_x$. A peri-

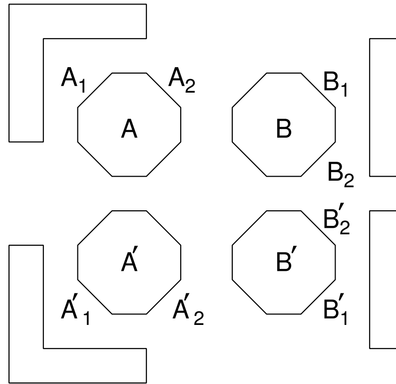

Figure 9.1: A feature is an object shape within a particular configuration of neighboring shapes. A and A' are the same feature if we identify edge A_1 with A_1' and A_2 with A_2'.

odic line feature is similarly determined by these four parameters:

$$\hat{O}_{\hat{x}}(\hat{x}) = \begin{cases} t_{\mathrm{bg}} & \text{if } |\hat{x} - n\hat{p}_x| \le \hat{d}/2, \quad n \in \mathbf{Z}, \\ t_{\mathrm{fg}} & \text{otherwise.} \end{cases} \tag{9.1}$$

The orientation of a feature does not constitute its environment. For example, a y-varying periodic line described by

$$\hat{O}_{\hat{y}}(\hat{y}) = \begin{cases} t_{\mathrm{bg}} & \text{if } |\hat{y} - n\hat{p}_y| \le \hat{d}/2, \quad n \in \mathbf{Z}, \\ t_{\mathrm{fg}} & \text{otherwise,} \end{cases}$$

is the same feature as that described by Eq. (9.1), provided they have the same t_{bg}, t_{fg}, and $\hat{d}$, and $\hat{p}_x = \hat{p}_y$.

With this understanding of "feature," we can define fluctuation as the variability of the same feature, and inherent variation as the difference, excluding fluctuation, between distinct features of the same object shape. Referring to Fig. 9.1, the difference between the delineated shapes of A and A' (and that between those of B and B') is fluctuation. So are differentiations between their delineated shapes across an exposure field, from wafer to wafer, and from lot to lot. The distinction between the averaged image of all replicas of A and A' (and those of B and B') is inherent variation.

By this demarcation, we can perceive fluctuations as arising from engineering imperfection while inherent variations as consequences of the laws of physics. The variation in the images of periodic spaces with the same nominal dimension $\hat{d}$ but different periodicities follows from Eq. (4.35) because of differences in their spectra. But no physical law dictates that images of a feature at two points in the field of an optical instrument should differ. The difference one may observe can be caused by aberration fluctuations of the imaging system.